Chemical Science

ROYAL SOCIETY OF CHEMISTRY

EDGE ARTICLE

View Article Online
View Journal | View Issue

Cite this: *Chem. Sci.*, 2023, **14**, 7913

All publication charges for this article have been paid for by the Royal Society of Chemistry

Received 12th April 2023
Accepted 20th June 2023

DOI: 10.1039/d3sc01921g

rsc.li/chemical-science

The proximity-enabled sulfur fluoride exchange reaction in the protein context†

Bingchen Yu, ‡ Li Cao,‡ Shanshan Li, Paul C. Klauser and Lei Wang *

The proximity-enabled sulfur(VI) fluoride exchange (SuFEx) reaction generates specific covalent linkages between proteins in cells and *in vivo*, which opens innovative avenues for studying elusive protein–protein interactions and developing potent covalent protein drugs. To exploit the power and expand the applications of covalent proteins, covalent linkage formation between proteins is the critical step, for which fundamental kinetic and essential properties remain unexplored. Herein, we systematically studied SuFEx kinetics in different proteins and conditions. In contrast to in small molecules, SuFEx in interacting proteins conformed with a two-step mechanism involving noncovalent binding, followed by covalent bond formation, exhibiting nonlinear rate dependence on protein concentration. The protein SuFEx rate consistently changed with protein binding affinity as well as chemical reactivity of the functional group and was impacted by target residue identity and solution pH. In addition, kinetic analyses of nanobody SR4 binding with SARS-CoV-2 spike protein revealed that viral target mutations did not abolish covalent binding but decreased the SuFEx rate with affinity decrease. Moreover, off-target cross-linking of a SuFEx-capable nanobody in human serum was not detected, and the SuFEx-generated protein linkage was stable at cellular acidic pHs, suggesting SuFEx suitability for *in vivo* usage. These results advanced our understanding of SuFEx reactivity and kinetics in proteins, which is invaluable for ongoing exploration of SuFEx-enabled covalent proteins for basic biological research and creative biotherapeutics.

Introduction

As a new generation of click chemistry,[1,2] sulfur(VI) fluoride exchange (SuFEx) has been widely used in small molecules in diverse fields such as chemical synthesis,[2,3] medicinal chemistry,[4–7] material chemistry[8,9] and chemical biology.[10,11] Aryl fluorosulfates and aryl sulfonyl fluorides are relatively latent towards biological nucleophiles, yet become reactive upon being placed in proximity to target protein residues, creating stable covalent linkages *via* SuFEx under cellular conditions.[1,11–13] This unique property drives the design and discovery of covalent small molecule inhibitors with therapeutic potentials.[5,6,14] Besides applications in small molecules, SuFEx has emerging power in proteins. For instance, it promoted the study of protein–protein interactions through cross-linking interacting protein pairs *in vivo*,[12,13,15] which preserves weak and transient protein–protein interactions for subsequent analysis. Recently, we demonstrated the concept of generating covalent protein drugs *via* proximity-enabled SuFEx between proteins *in vivo*.[13,15,16] In this strategy, latent bioreactive unnatural amino acids (Uaas) carrying aryl fluorosulfate or sulfonyl fluoride groups are site-specifically incorporated into protein drugs *via* genetic code expansion. These Uaas include fluorosulfate-L-tyrosine (FSY),[13] fluorosulfonyloxybenzoyl-L-lysine (FSK),[15] *meta*-fluorosulfate-L-tyrosine (mFSY),[17] fluorine-substituted fluorosulfate-L-tyrosine (FFY),[18] and *o*-sulfonyl fluoride-*O*-methyltyrosine (SFY).[19,20] Upon binding with the target protein, these Uaas can crosslink with Lys, His or Tyr on the target *via* SuFEx to form a stable covalent linkage between the drug and target proteins. Covalent protein drugs were firstly demonstrated *in vivo* on a programmed cell death protein-1 (PD-1)/PD-L1 pair, where FSY was incorporated into PD-1 to covalently block PD-L1, exhibiting potent antitumor efficacy over the noncovalent wildtype PD-1.[21] This strategy has been subsequently used to build covalent antibodies for human rhinovirus 14 (HRV14) 3C protease,[22] covalent protein inhibitors for neutralizing SARS-CoV-2,[18,23] and covalent protein radiopharmaceuticals to enhance efficacy and safety for targeted radionuclide therapies,[24] showing great potential in developing novel biotherapeutics.

For various emerging SuFEx applications in proteins, the formation of the protein–protein covalent linkage is a key step. SuFEx kinetics determines the covalent bond formation rate and would thus directly impact the efficacy. Although SuFEx kinetics has been characterized on small molecules,[25] it has not

Department of Pharmaceutical Chemistry, The Cardiovascular Research Institute, Helen Diller Family Comprehensive Cancer Center, University of California San Francisco, 555 Mission Bay Blvd. South, San Francisco, California 94158, USA. E-mail: Lei.wang2@ucsf.edu

† Electronic supplementary information (ESI) available. See DOI: https://doi.org/10.1039/d3sc01921g

‡ Contributed equally.

been systematically studied in the protein–protein context. Chemical reactivity and kinetics can differ significantly at the level of small molecules from proteins.[1,26–28] For instance, target-specific covalent small molecule inhibitors have been shown to inhibit proteins in a generic two-step mechanism involving non-covalent complex formation followed by covalent reaction.[29] Here we report a systematic investigation of SuFEx kinetic and essential properties in the protein–protein context. We found that SuFEx kinetics in the protein–protein context conformed with a two-step mechanism, which is different from kinetics on small molecules but analogous to that of covalent small molecules inhibiting their target protein. Protein–protein SuFEx showed nonlinear dependence of protein concentrations, the rate of which was affected by protein binding affinity, chemical reactivity of the functional group, target residue identity, and pH. We further studied the important practical properties of SuFEx in proteins, including the impact of target mutations, off-target reactivity, and linkage stability. These results will be highly valuable in guiding the innovative use of SuFEx for studying and engineering proteins in covalent chemical mode. The general kinetic principles revealed for covalent linkage formation between proteins should further inspire the development of new proximity-enabled chemistry for biocompatible usage *in vivo*.

Results and discussion

Protein–protein covalent linkage formation *via* proximity-enabled reactivity

Covalent linkage formation between two interacting proteins through proximity-enabled reactivity generally occurs in two steps (Scheme 1): the two proteins first bind forming a non-covalent complex, which places the latent bioreactive Uaa of one protein close to a target natural residue of the other protein.[30] Accelerated by the proximity effects, the latent Uaa and its target residue then undergo reaction, giving rise to a specific covalent linkage. The initial non-covalent binding of the two proteins is governed by their affinity (K_i), and the subsequent covalent bond formation is determined by the covalent reaction rate k_2. The reaction under study in this work is SuFEx, for which the latent bioreactive Uaa is FSY carrying the fluorosulfonate group and its target natural residue can be Lys, His, or Tyr. Fluorosulfonate undergoes the SuFEx reaction with the nucleophilic side chains of these natural residues when placed in close proximity. Owing to the two-step mechanism, we expect that the kinetics for such protein–protein covalent linkage formation would be different from the second-order kinetics for two reacting small molecules, in which the reaction rate keeps increasing with reactant concentrations. Instead, we expect that the kinetics would be analogous to that of an irreversible small molecule inhibitor acting on its target protein. We tested this kinetic hypothesis using different binding protein pairs and SuFEx-capable functional groups.

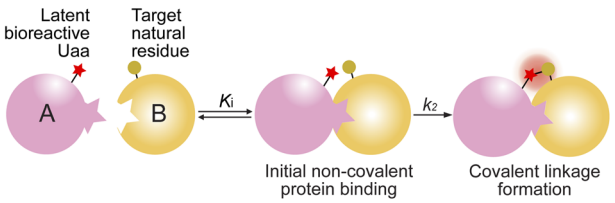

Scheme 1 Covalent linkage formation between interacting proteins *via* proximity-enabled reactivity.

SuFEx kinetics in the Z_{spa} affibody–Z protein pair

We began with an affibody-target protein pair to study the kinetics of SuFEx in the protein context. The Z_{spa} affibody (Afb) binds with its target Z protein with a K_d of ~6 μM.[31] On the basis of the crystal structure of the Afb-Z complex,[31] the latent bioreactive Uaa FSY was incorporated at site 24 of the Z protein to covalently target Lys7 of the Afb (Fig. 1A).[13] The FSY incorporation and target sites were selected based on their average distance and side chain orientation so that the side chains could contact when the two proteins bind. Maltose binding protein (MBP) was fused to the N-terminus of the Z protein generating the MBP-Z fusion protein to better separate the Z

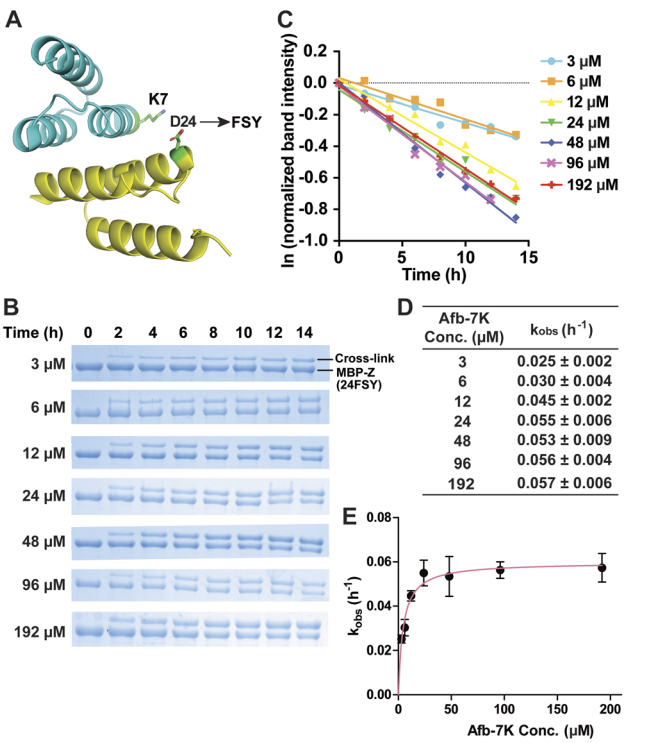

Fig. 1 Measurement of SuFEx kinetics in the Z_{spa} affibody–Z protein pair. (A) Crystal structure of the Z_{spa} affibody (Afb, cyan) binding with the Z protein (yellow), with residue Asp24 for FSY incorporation and target Lys7 shown in sticks. (B) SDS-PAGE analysis of cross-linking of 6 μM MBP-Z(24FSY) with different concentrations of Afb *in vitro* for the indicated duration of incubation time. (C) Determination of the pseudo-first-order rate constant k_{obs} for different concentrations of Afb. The experiments were independently repeated three times, and the data for one time are shown here. (D) Calculated k_{obs} for each Afb concentration. Mean ± s.d., $n = 3$. (E) Plotting k_{obs} against Afb concentration [Afb] to determine the second-order rate constant k. The data were fitted to equation $k_{obs} = k_{max}[Afb]/(K_S + [Afb])$. Error bars represent s.d., $n = 3$.

protein from the Afb, which have similar molecular weights. MBP-Z(24FSY) and Afb were expressed in *E. coli* and affinity purified through the Hisx6-tag appended at their C-termini.

We first tested the stability of proteins containing FSY in aqueous buffer. MBP-Z(24FSY) was incubated in PBS (pH = 7.4) at 37 °C for 24 h and analyzed with high resolution electrospray ionization time-of-flight mass spectrometry (ESI-TOF MS). The protein's MS peak did not change before and after incubation (Fig. S1†). Similar results were also obtained with another protein, in which FSY was incorporated into site 6 of ubiquitin (Fig. S2†). These results indicate that FSY was stable in proteins under the tested conditions.

Next, 6 μM MBP-Z(24FSY) was incubated with Afb ranging from 3 to 192 μM in phosphate-buffered saline (PBS, pH 7.4) at 37 °C. At different time points, samples were extracted, quenched with 4% SDS, and analyzed with SDS-PAGE under denatured conditions. At all concentrations, we observed a time-dependent decrease of MBP-Z(24FSY) band intensity and a concomitant increase of cross-link band intensity (Fig. 1B).

To determine the kinetics of covalent protein complex formation, we measured the MBP-Z(24FSY) band intensities and normalized the band intensities at different time points relative to the band intensity at 0 h (before cross-linking). The natural logarithm (ln) of the normalized MBP-Z(24FSY) band intensity was plotted against time. For each Afb concentration tested, a linear relationship was observed in the plot with $R^2 > 0.95$ in most cases (Fig. 1C and S3†). The pseudo-first-order rate constant, k_{obs}, was calculated for each concentration (Fig. 1D), and was plotted against Afb concentration in Fig. 1E. The k_{obs} for covalent protein complex formation initially increased with increasing concentration of Afb and then reached a plateau at around 24 μM Afb, exhibiting a hyperbolic dependence that saturated at a maximum rate constant of $k_{max} = 0.0597 \pm 0.0019$ h^{-1}. The half-saturating concentration K_S, the concentration needed to reach half of the maximum reaction rate, of Afb was calculated to be 4.5 μM. Therefore, the second-order rate constant, $k = k_{max}/K_S$,[29,32] for covalent protein complex formation was determined to be $(1.32 \pm 0.04) \times 10^4$ M^{-1} h^{-1}.

SuFEx kinetics in the nanobody 7D12–EGFR pair

The proximity-enabled SuFEx reaction between proteins is driven by the binding of the two proteins, which places the latent bireactive Uaa in close proximity to its target natural residue. We thus expect that the protein binding affinity could play a critical role in the SuFEx kinetics. To investigate this effect, we further studied the SuFEx kinetics using the 7D12 nanobody, which binds to the human epidermal growth factor receptor (EGFR) with a K_d of 200 nM.[33] Its binding affinity is higher than that of the Afb–Z protein pair ($K_d = 6$ μM).

On the basis of the crystal structure of the 7D12–EGFR complex,[33] FSY was incorporated at site 109 of the 7D12 nanobody [7D12(109FSY)] to covalently target Lys443 of the EGFR (Fig. 2A).[15] The mutant nanobody 7D12(109FSY) was expressed in *E. coli* and affinity purified through the Hisx6 tag appended at the C-terminus. We then incubated 0.2 μM EGFR with 7D12(109FSY) ranging from 0.2 to 12.8 μM in PBS (pH 7.4) at

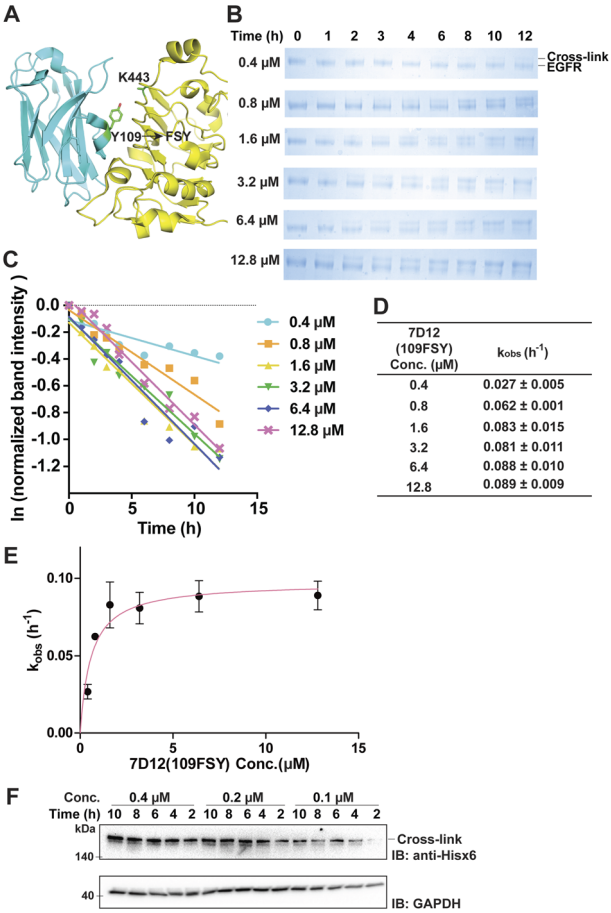

Fig. 2 Measurement of SuFEx kinetics in the nanobody 7D12–EGFR pair. (A) Crystal structure of nanobody 7D12 (cyan) binding with the human EGFR (yellow), with residue Tyr109 for FSY incorporation and target Lys443 shown in sticks. (B) SDS-PAGE analysis of cross-linking of 0.2 μM EGFR with different concentrations of 7D12(109FSY) *in vitro* for the indicated duration of incubation time. (C) Determination of the pseudo-first-order rate constant k_{obs} for different concentrations of 7D12(109FSY). The experiments were independently repeated three times, and the data for one time are shown here. (D) Calculated k_{obs} for each 7D12(109FSY) concentration. Mean ± s.d., $n = 3$. (E) Plotting k_{obs} against 7D12(109FSY) concentration [7D12] to determine the second-order rate constant k. The data were fitted to equation $k_{obs} = k_{max}[7D12]/(K_S + [7D12])$. Error bars represent s.d., $n = 3$. (F) Cross-linking of 7D12(109FSY) with the EGFR on the cell surface. Cells were incubated with varying concentrations of 7D12(109FSY) for the indicated time period, after which cell lysates were analyzed by denatured western blot to detect the cross-linked EGFR–7D12 complex. GAPDH was detected as the loading control.

37 °C. Samples were extracted, quenched, and analyzed with SDS-PAGE at different incubation time points. The extracellular domain of the EGFR with an Fc tag (total MW = 95 kDa), instead of a full-length EGFR (MW = 200 kDa), was used in these *in vitro* cross-linking experiments, so that the cross-linked EGFR could be clearly separated from the non-cross-linked EGFR by gel electrophoresis. When 0.2 μM 7D12(109FSY) was used, the cross-linking band was not obvious until 10 h, suggesting that the cross-linking rate was low at this concentration. At other 7D12(109FSY) concentrations, a time-dependent decrease of

EGFR band intensities and concomitant increase of cross-link band intensities were detected (Fig. 2B).

Plotting the normalized EGFR band intensity against time also showed a linear relationship with $R^2 > 0.90$ in most cases (Fig. 2C and S4†). The pseudo-first-order rate constant, k_{obs}, was calculated for each concentration of 7D12(109FSY) (Fig. 2D) and plotted against 7D12(109FSY) concentration (Fig. 2E). Similar to what was observed in the Afb–Z protein pair, the k_{obs} for covalent 7D12(109FSY)–EGFR complex formation initially increased with increasing concentration of 7D12(109FSY) and then reached a plateau, displaying a hyperbolic dependence. The k_{max} was calculated to be 0.0972 ± 0.0054 h^{-1} and K_S 0.58 μM, giving a second-order rate constant k of (1.68 ± 0.09) × 10^5 M^{-1} h^{-1}.

Protein SuFEx kinetics and effects of binding affinity

In both protein pairs, we observed that the protein SuFEx rate initially increased with protein concentration when protein concentration was low and then reached a maximum rate despite further increase of protein concentration. These results are consistent with the two-step mechanism (Scheme 1) for protein–protein covalent linkage formation *via* proximity-enabled reactivity and confirmed our kinetics hypothesis. When both protein concentrations are low (≤K_d), a significant amount of protein is not bound, limiting the SuFEx rate; an increase of protein concentration promotes protein association and increases the SuFEx rate. When one protein is supplied in high concentration (>several-fold of K_d), the majority of the other protein has already been bound, and further increase of the former will no longer significantly increase the SuFEx rate, resulting in the observed rate plateau.

A comparison of SuFEx kinetics in the above two protein pairs reveals the effect of the binding affinity of the proteins. For the Afb–Z protein pair with a lower binding affinity, the maximum k_{obs} was 0.0597 ± 0.0019 and was reached when MBP-Z(24FSY) and Afb-7K concentrations were 6 μM and 24 μM, respectively. The calculated second-order rate constant was (1.32 ± 0.04) × 10^4 M^{-1} h^{-1}. For the 7D12–EGFR pair with a higher binding affinity, the maximum k_{obs} was 0.0972 ± 0.0054 h^{-1} and was reached when EGFR and 7D12(109FSY) concentrations were 0.2 μM and 1.6 μM, respectively. The calculated second-order rate constant was (1.68 ± 0.09) × 10^5 M^{-1} h^{-1}, ten-times higher than that of the Afb–Z protein pair. Therefore, a higher binding affinity resulted in a faster apparent second-order SuFEx rate between proteins.

SuFEx kinetics of the nanobody 7D12 cross-linking endogenous EGFR on the cell surface

Aside from purified proteins binding *in vitro*, we also evaluated SuFEx kinetics on native proteins expressed on the live cell surface, which represents a general application setting of covalent protein binders or therapeutics. Specifically, EGFR-expressing A431 cells were incubated with varying concentrations of 7D12(109FSY) for the indicated time period, after which cell lysates were analyzed with western blot under denatured conditions to detect the EGFR cross-linked by the nanobody 7D12(109FSY). Ideally, an EGFR-specific antibody should be used to detect both the cross-linked and non-cross-linked EGFRs in order to quantitate the kinetics. However, the full-length native EGFR on cells has a large molecule weight (MW) of 200 kDa, making it difficult to clearly separate it from the EGFR cross-linked by 7D12(109FSY) (MW = 215 kDa). As a result, we used an anti-Hisx6 antibody to detect the Hisx6 tag appended at the C-terminus of 7D12(109FSY) so as to visualize the cross-linked EGFR–7D12(109FSY) complex.

As shown in Fig. 2F, the cross-linking bands intensified with the increase of incubation time. On the basis of the band intensities, when 7D12(109FSY) concentration increased from 0.1 μM to 0.2 μM, the cross-linking rates increased; however, no significant rate increase was observed when a higher concentration (0.4 μM) was used. Further increasing concentration of 7D12(109FSY) from 0.4 μM to 3.2 μM did not further increase the cross-link rates (Fig. S5†). These results indicate that the SuFEx rate on the cell surface also increased with increasing concentration of 7D12(109FSY) and plateaued around 0.2 μM. Interestingly, the SuFEx rate for 7D12(109FSY)–EGFR on the cell surface reached the plateau at a lower 7D12(109FSY) concentration (0.2 μM) than that *in vitro* (1.6 μM). The EGFR is known to cluster on the cell surface, which can enhance the local effective concentration and contribute to this difference.

Effects of chemical reactivity on protein SuFEx kinetics

Besides the fluorosulfonate group, the sulfonyl fluoride group is another latent bioreactive functional group that can react through SuFEx.[1,2,34] In the protein–protein context, both fluorosulfonate and sulfonyl fluoride can form stable linkages with side chains of His, Lys, and Tyr, but their resultant linkages with the side chains of Cys, Ser, and Thr are unstable.[13,20,25,35,36] From the chemical point of view, sulfonyl fluoride is considered to be more reactive than fluorosulfonate.[25,37] Since the second step of the proximity-enabled SuFEx reaction between proteins directly involves reactivity, we thus evaluated how intrinsic chemical reactivity impacts protein SuFEx kinetics. We recently designed and genetically encoded the Uaa *o*-sulfonyl fluoride-*O*-methyltyrosine (SFY), which bears a sulfonyl fluoride group. SFY is able to crosslink proteins with different types of biomolecules including proteins, carbohydrates, and RNA.[19,20] The sulfonyl fluoride group in SFY is located at the *meta* position of the phenyl ring, while FSY has the fluorosulfonate group at the *para* position. We have shown that the orientation of the functional group affects the reactivity in the proximity-enabled SuFEx reaction on proteins.[17,34] Therefore, we decided to compare SFY with mFSY, whose fluorosulfonate group is also at the *meta* position (Fig. 3A).[17]

We compared the SuFEx kinetics of mFSY and SFY using *E. coli* glutathione transferase (ecGST), a homodimeric protein. On the basis of the crystal structure of ecGST,[38] mFSY or SFY was incorporated into site 103 of ecGST at the dimer interface to target Lys107 of the other monomer.[39] ecGST(103mFSY) and ecGST(103SFY) were separately expressed in *E. coli* cells. At different time points after the induction of ecGST expression, *E. coli* cells were extracted, and cell lysates were analyzed by denatured western blot to detect the covalent dimerization of

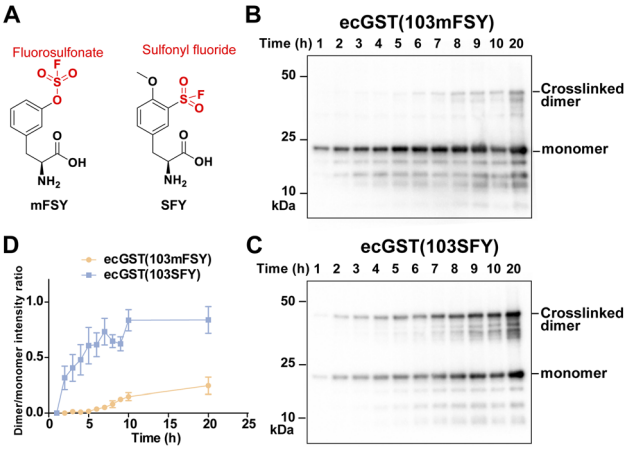

Fig. 3 SuFEx kinetics comparison between fluorosulfonate and sulfonyl fluoride in ecGST. (A) Structure of SFY and mFSY bearing sulfonyl fluoride and fluorosulfonate groups, respectively. (B and C) Covalent dimerization of ecGST(103mFSY) (B) and ecGST(103SFY) (C) at different time points in *E. coli* cells. The experiments were independently repeated three times, and the data for one time are shown here. (D) Band intensity ratio of ecGST crosslinked dimer to monomer at different time points. $n = 3$ independent repeats; error bars represent s.e.m.

ecGST. As shown in Fig. 3B–D, ecGST(103SFY) exhibited a much faster covalent dimerization rate than ecGST(103mFSY), suggesting that sulfonyl fluoride affords a faster SuFEx reaction rate than fluorosulfonate in this protein context.

Effects of target residue identity and pH on protein SuFEx kinetics

Previously we demonstrated that FSY can crosslink with Lys, His, or Tyr through SuFEx in various proteins. Here we systematically compared the SuFEx kinetics of FSY with these different target residues in the context of the Afb–Z protein pair. We incubated 6 μM MBP-Z(24FSY) with 192 μM Afb-7K, Afb-7H, or Afb-7Y in PBS (pH 7.4) at 37 °C. At different time points, samples were extracted, quenched, and analyzed with SDS-PAGE under denatured conditions. An excess of Afb was used to measure the maximum SuFEx rate. As shown in Fig. 4A, Afb-7K, Afb-7H, and Afb-7Y all cross-linked with MBP-Z(24FSY) in a time-dependent manner. We quantified the MBP-Z(24FSY) band intensities and calculated the k_{obs} using the same method described above (Fig. 4B and S6†). Under these conditions, the maximum SuFEx rate (k_{obs}) for Afb-7H, Afb-7K, and Afb-7Y with FSY was 0.110 ± 0.001 h^{-1}, 0.057 ± 0.006 h^{-1}, and 0.022 ± 0.007 h^{-1}, respectively (Fig. 4C). The binding affinity between WT MBP-Z and Afb-7K, 7H, or 7Y was measured with biolayer interferometry, which showed slight differences and a trend opposite to that of k_{obs} (Fig. S7†), suggesting that the mutation effect on binding affinity was not the main drive of the k_{obs} difference. Afb-7H exhibited the fastest SuFEx rate possibly because the histidine side chain has the lowest pK_a and thus the most efficient deprotonation.

We next incubated 192 μM Afb and 6 μM MBP-Z(24FSY) in Tris buffer (pH 8.8) at 37 °C to study the effects of pH on SuFEx kinetics (Fig. 4D and S8†). Afb-7K cross-linked with MBP-Z(24FSY) at pH 8.8 quite fast, so a narrower time range (0 to 5 h) was used to improve the accuracy of measurement. A more basic pH increased the SuFEx rate for all three residues, but to varying extents. Afb-7K cross-linked with MBP-Z(24FSY) about 5-times faster at pH 8.8 than at pH 7.4; Afb-7Y was 3.5-fold faster; Afb-7H had just a slight rate increase (Fig. 4C). Interestingly, while Afb-7H showed the fastest SuFEx k_{obs} rate with FSY at pH 7.4, Afb-7K had the fastest SuFEx k_{obs} rate at pH 8.8.

We selected the Afb–Z protein pair to study the pH effect because the incorporated FSY and its target residue are both at the surface of the protein complex, making them more amenable to pH change of the solution. For Uaa-target residue located in a protein microenvironment that can resist external pH change, adjusting solution pH may or may not impact the SuFEx kinetics.

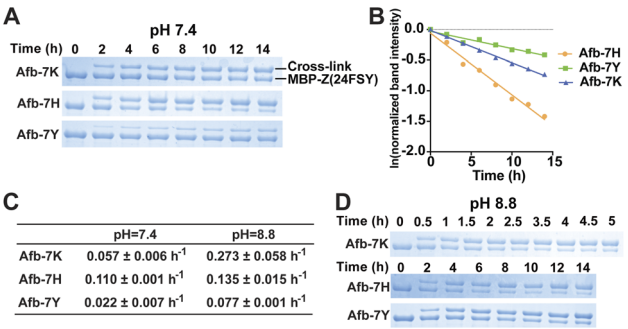

Fig. 4 Effects of the target residue identity and pH on SuFEx kinetics in the Afb–Z protein pair. (A) SDS-PAGE analysis of cross-linking of 6 μM MBP-Z(24FSY) with 192 μM Afb-7K, Afb-7H, or Afb-7Y at pH 7.4 *in vitro* at different time points. (B) Determination of maximum k_{obs} between MBP-Z(24FSY) and different Afb at pH 7.4. The experiments were independently repeated three times, and the data for one time are shown here. (C) Calculated maximum k_{obs} between MBP-Z(24FSY) and different Afb at pH 7.4 and 8.8 (mean ± s.d., $n = 3$). (D) SDS-PAGE analysis of cross-linking of 6 μM MBP-Z(24FSY) with 192 μM Afb-7K, Afb-7H, or Afb-7Y at pH 8.8 *in vitro* at different time points.

Effects of target mutation on protein SuFEx kinetics

An emerging application of proximity-enabled reactivity is the development of covalent protein drugs, target of which may undergo mutation during treatment and disease progression. Such mutations may alter the binding affinity of the protein drug and the kinetics of covalent linkage formation between the protein drug and its target, thus affecting the drug efficacy. We therefore evaluated the influence of target protein mutations on SuFEx kinetics in the protein context.

Utilizing the proximity-enabled SuFEx reaction, we recently developed covalent nanobodies to neutralize SARS-CoV-2.[18] FSY was incorporated into nanobodies and the resultant nanobodies covalently bind with the receptor binding domain (RBD) of the spike protein of SARS-CoV-2, thus blocking the binding of SARS-CoV-2 to the human ACE2 receptor, a critical step for SARS-CoV-2 infection. Various mutated SARS-CoV-2 strains have emerged in the pandemic. Mutations on the spike RBD such as

E484K, F490L and N439K have been shown to decrease affinity towards neutralization antibodies;[40–42] The B.1.1.7 lineage, which mainly possesses N501Y mutation, shows a stronger interaction with ACE2 and a faster spreading rate;[43] The B.1.351 lineage, which has K417N, E484K, and N501Y mutations on the spike RBD, has decreased affinity towards neutralization antibodies and can lower the effectiveness of current vaccine.[44–46] It is thus important to study the SuFEx kinetics of the covalent nanobodies with the mutant spike RBD to evaluate the therapeutic potential of covalent nanobodies in fighting against evolving infectious diseases.

On the basis of the structure of the SARS-CoV-2 spike RBD in complex with nanobody SR4,[47] we incorporated FSY into site 57 of nanobody SR4 to target Tyr505 of the spike RBD and demonstrated that SR4(57FSY) covalently cross-linked with the wildtype (WT) spike RBD. To assess affinity change caused by SARS-CoV-2 mutation, we then determined the dissociation constant (K_d) between the WT SR4 nanobody and the WT or mutant spike RBD using biolayer interferometry (BLI). As shown in Fig. 5A, all mutated spike RBDs had decreased affinity toward the SR4 nanobody. To measure the cross-linking rates between SR4(57FSY) and various spike RBDs, we next incubated 5 μM SR4(57FSY) with 0.5 μM different spike RBDs at 37 °C in PBS. At different time points, an aliquot was extracted and the cross-linking between SR4(57FSY) and spike RBDs was detected with western blot.

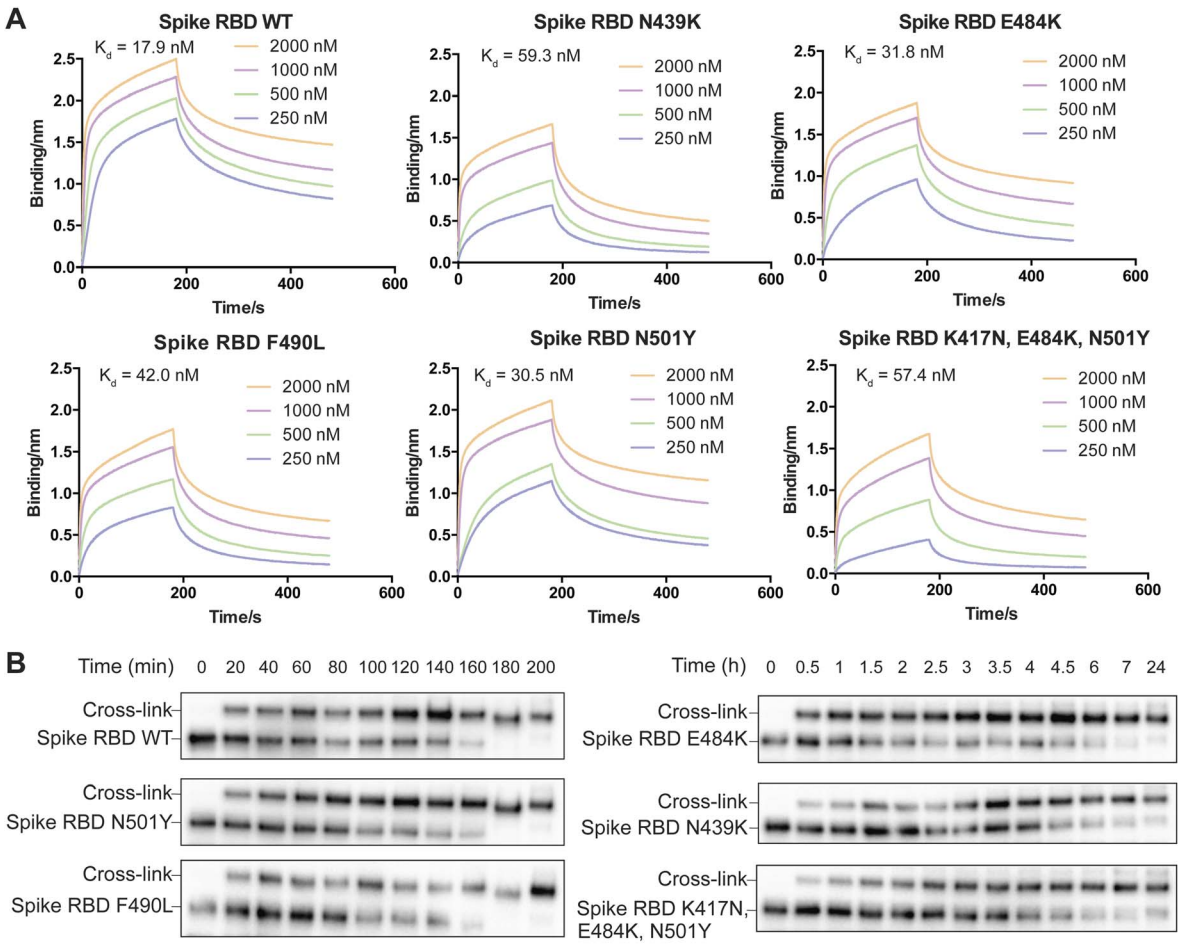

C

Spike RBD	K_d (nM)	k_{on} (1/Ms)	k_{off} (1/s)	k_{obs} (h^{-1}) (n=3)
WT	17.9	1.26×10^5	2.26×10^{-3}	0.595 ± 0.013
N501Y (Alpha)	30.5	8.86×10^4	2.70×10^{-3}	0.608 ± 0.088
F490L	42	1.13×10^5	4.76×10^{-3}	0.392 ± 0.083
N439K	59.3	1.00×10^5	5.95×10^{-3}	0.236 ± 0.023
E484K	31.8	1.07×10^5	3.40×10^{-3}	0.314 ± 0.010
K417N, E484K, and N501Y (Beta)	57.4	7.08×10^4	4.06×10^{-3}	0.291 ± 0.021

Fig. 5 Effects of target mutation on SuFEx kinetics in nanobody SR4(57FSY) cross-linking SARS-CoV-2 spike RBDs. (A) Biolayer interferometry assay of the dissociation constant K_d between the WT SR4 nanobody and WT or mutant spike RBDs. (B) Western blot analysis of cross-linking of SR4(57FSY) with WT or mutant spike RBDs. An anti-Hisx6 antibody was used to detect the Hisx6 tag appended at the C-terminus of the spike RBD. (C) The binding and kinetic constants measured between nanobody SR4(57FSY) and WT or mutant spike RBDs.

SR4(57FSY) was still able to form covalent adducts with all five mutant spike RBDs efficiently (Fig. 5B). We quantified the spike RBD band intensities and calculated the k_{obs} (Fig. 5C). The results indicate that the SuFEx rate k_{obs} generally decreased when the binding affinity between SR4(57FSY) and spike RBDs decreased. One exception is the N501Y mutant spike RBD, which cross-linked with SR4(57FSY) at a similar rate to the WT spike RBD. It is worth noting that the influence of binding affinity on the SuFEx rate was not necessarily linear. We reason that the cross-linking rate would also be affected by mutation-induced protein conformation and microenvironment change surrounding the FSY-target residue, which warrants further studies.

Covalent specificity of FSY-incorporated protein

A critical concern for covalent drugs is the reaction specificity, as off-target covalent reactions could result in toxicity in cells and *in vivo*. The covalent reactivity of the proximity-enabled reaction in proteins entails (1) the specific binding of the protein drug toward the target and (2) the proper contact of the latent bioreactive Uaa with a suitable target natural residue of the bound protein. This dual requirement is expected to safeguard the reaction specificity of the protein drug toward its target. To evaluate the covalent specificity of SuFEx capable proteins, we tested whether FSY-incorporated protein would lead to off-target cross-linking of other proteins. Specifically, we incubated 0.5 mg mL^{-1} 7D12(109FSY) in 50% human serum at 37 °C. At different time points, samples were aliquoted and 7D12(109FSY) was pulled down *via* the C-terminal Hisx6 tag and then analyzed with SDS-PAGE and western blot to examine if any off-target proteins were non-specifically cross-linked. The noncovalent WT 7D12 was used as the control.

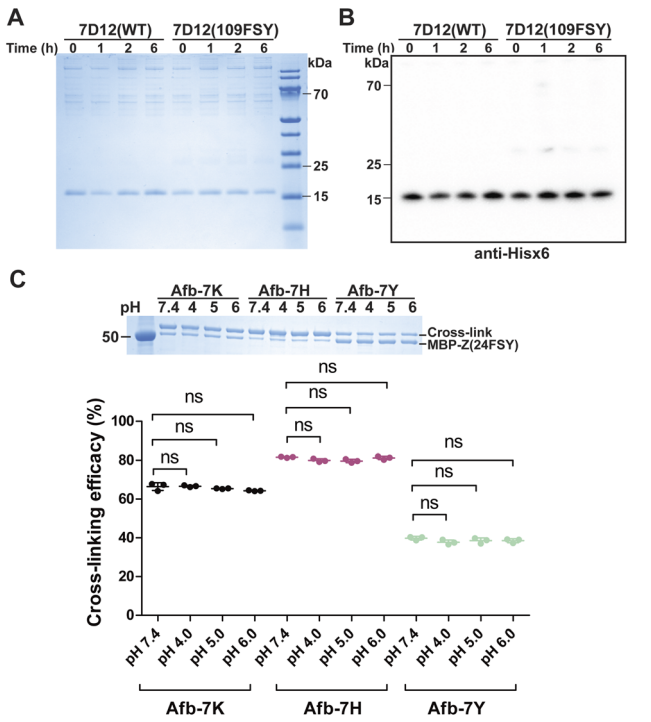

Fig. 6 Covalent specificity in human serum and stability of the protein linkage at acidic pH. (A and B) SDS-PAGE (A) and western blot (B) analyses of 7D12(109FSY) and 7D12(WT) after incubation in 50% human serum at 37 °C for the indicated time duration. (C) SDS-PAGE analysis of the stability of the covalent linkage generated between MBP-Z(24FSY) and Afb-7X by FSY reacting with Lys, His, or Tyr. The cross-linked protein samples were incubated at different pH (4, 5, and 6) for 24 h followed by SDS-PAGE analysis. The cross-linking efficacy (%) was quantified as the cross-linking band intensity/[MBP-Z(24FSY) band intensity + cross-link band intensity]. Error bars represent s.d.; $n = 3$ independent experiments; ns, not significant.

As shown in Fig. 6A, aside from the 7D12 nanobody band, several other bands with higher molecular weights were also observed. However, these bands also showed up in the WT 7D12 control, which is incapable of forming covalent bonds. In addition, the intensity of these bands did not increase with the incubation time, which further ruled out that these bands were derived from covalent cross-linking of 7D12(109FSY). Moreover, in the western blot in which an anti-Hisx6 antibody was used to detect the Hisx6 tag appended at the C-terminus of 7D12 (Fig. 6B), these bands were not detectable, further indicating that they did not contain 7D12(109FSY). A very faint band was observed in western blot at the position matching the dimer of 7D12, whose intensity was less than 2% of 7D12(109FSY). The 7D12 nanobody has a dimerization tendency, so we suspected that this faint band was from the 7D12(109FSY) covalent dimer, formation of which was facilitated by the high temperature during sample preparation (95 °C and 10 min) for western blot. Because the intensity of this band also did not increase with the incubation time, this band could not be from non-specific cross-linking of 7D12(109FSY) with other serum proteins. In short, these results indicate that 7D12(109FSY) did not result in non-specific cross-linking of off-target proteins in human serum in the time period studied, suggesting high covalent specificity.

Stability of the protein linkage generated by FSY

Another important practical consideration is the stability of the covalent protein linkage generated by SuFEx, as the covalent protein complex may be internalized inside cells and traffic through the acidic endosomal pathway. We therefore evaluated the stability of the FSY-generated protein covalent linkages at acidic pHs. Specifically, 0.3 mg mL^{-1} MBP-Z(24FSY) was incubated with 1 mg mL^{-1} Afb-7X (X = K, Y or H) at 37 °C in PBS (pH 7.4) for 12 h to allow cross-linking. Protein samples were then exchanged into citrate-phosphate buffer with different pH (4, 5, and 6) and incubated for 24 h to test linkage stability, followed by SDS-PAGE analysis. As shown in Fig. 6C, compared with pH 7.4, the cross-linking efficacy of MPB-Z(24FSY) with Afb did not change after incubation at pH 4, 5, or 6, which held for all three linkages generated between FSY and Lys, His, and Tyr, indicating that the FSY-generated covalent protein linkage remained stable at these acidic pHs for the tested duration.

Conclusions

In summary, the SuFEx kinetics for protein–protein covalent linkage formation *via* proximity-enabled reactivity conformed

with a two-step mechanism involving protein binding followed by covalent bond formation, showing nonlinear dependence of protein concentration. This kinetics is different from that of the biomolecular reaction of small molecules but analogous to that of covalent small molecules inhibiting target protein. The reaction rate consistently increased with the protein binding affinity and chemical reactivity of the functional group. Target residue identity as well as pH also affected the reaction rate. Mutations in target protein that decreased binding affinity led to decreasing SuFEx rate but in a nonlinear manner. The covalent nanobody based on SuFEx reactivity showed no off-target cross-linking in human serum, and the SuFEx-generated covalent protein linkage remained stable at cellular acidic pHs, suggesting SuFEx suitability for *in vivo* applications. These results filled the gap of understanding SuFEx reactivity and kinetics in the protein–protein context, which will be invaluable to guide ongoing exploration of SuFEx in proteins *in vivo* for basic biological studies and innovative covalent biotherapeutics.

Data availability

All related data have been included in the paper and the ESI file.†

Author contributions

The study was designed and conceptualized by BY, LC, SL and LW. Kinetic and stability studies were performed by BY. Cellular cross-link studies were conducted by LC and SL. mFSY was synthesized by PK. The results were discussed and interpreted by BY, LC, SL, PK and LW. The manuscript was written by BY and LW with input from the other authors.

Conflicts of interest

There are no conflicts to declare.

Acknowledgements

L. W. acknowledges the support of the NIH (R01GM118384 and R01CA258300).

Notes and references

1 A. S. Barrow, C. J. Smedley, Q. Zheng, S. Li, J. Dong and J. E. Moses, *Chem. Soc. Rev.*, 2019, **48**, 4731–4758.
2 J. Dong, L. Krasnova, M. G. Finn and K. B. Sharpless, *Angew. Chem., Int. Ed.*, 2014, **53**, 9430–9448.
3 B. Gao, S. Li, P. Wu, J. E. Moses and K. B. Sharpless, *Angew. Chem., Int. Ed.*, 2018, **57**, 1939–1943.
4 S. Kitamura, Q. Zheng, J. L. Woehl, A. Solania, E. Chen, N. Dillon, M. V. Hull, M. Kotaniguchi, J. R. Cappiello, S. Kitamura, V. Nizet, K. B. Sharpless and D. W. Wolan, *J. Am. Chem. Soc.*, 2020, **142**, 10899–10904.
5 Q. Zhao, X. Ouyang, X. Wan, K. S. Gajiwala, J. C. Kath, L. H. Jones, A. L. Burlingame and J. Taunton, *J. Am. Chem. Soc.*, 2017, **139**, 680–685.
6 Z. Liu, J. Li, S. Li, G. Li, K. B. Sharpless and P. Wu, *J. Am. Chem. Soc.*, 2018, **140**, 2919–2925.
7 Y. You, H. S. Kim, I. H. Bae, S. G. Lee, M. H. Jee, G. Keum, S. K. Jang and B. M. Kim, *Eur. J. Med. Chem.*, 2017, **125**, 87–100.
8 B. Gao, L. Zhang, Q. Zheng, F. Zhou, L. M. Klivansky, J. Lu, Y. Liu, J. Dong, P. Wu and K. B. Sharpless, *Nat. Chem.*, 2017, **9**, 1083–1088.
9 K. Durie, J. Yatvin, M. Kovaliov, G. H. Crane, J. Horn, S. Averick and J. Locklin, *Macromolecules*, 2018, **51**, 297–305.
10 A. Narayanan and L. H. Jones, *Chem. Sci.*, 2015, **6**, 2650–2659.
11 P. Martín-Gago and C. A. Olsen, *Angew. Chem., Int. Ed.*, 2019, **58**, 957–966.
12 B. Yang, H. Wu, D. Schnier Paul, Y. Liu, J. Liu, N. Wang, F. DeGrado William and L. Wang, *Proc. Natl. Acad. Sci. U. S. A.*, 2018, **115**, 11162–11167.
13 N. Wang, B. Yang, C. Fu, H. Zhu, F. Zheng, T. Kobayashi, J. Liu, S. Li, C. Ma, P. G. Wang, Q. Wang and L. Wang, *J. Am. Chem. Soc.*, 2018, **140**, 4995–4999.
14 D. E. Mortenson, G. J. Brighty, L. Plate, G. Bare, W. Chen, S. Li, H. Wang, B. F. Cravatt, S. Forli, E. T. Powers, K. B. Sharpless, I. A. Wilson and J. W. Kelly, *J. Am. Chem. Soc.*, 2018, **140**, 200–210.
15 J. Liu, L. Cao, P. C. Klauser, R. Cheng, V. Y. Berdan, W. Sun, N. Wang, F. Ghelichkhani, B. Yu, S. Rozovsky and L. Wang, *J. Am. Chem. Soc.*, 2021, **143**, 10341–10351.
16 N. Wang and L. Wang, *Curr. Opin. Chem. Biol.*, 2022, **66**, 102106.
17 P. C. Klauser, V. Y. Berdan, L. Cao and L. Wang, *Chem. Commun.*, 2022, **58**, 6861–6864.
18 B. Yu, S. Li, T. Tabata, N. Wang, L. Cao, G. R. Kumar, W. Sun, J. Liu, M. Ott and L. Wang, *Chem*, 2022, **8**, 2766–2783.
19 S. Li, N. Wang, B. Yu, W. Sun and L. Wang, *Nat. Chem.*, 2023, **15**, 33–42.
20 W. Sun, N. Wang, H. Liu, B. Yu, L. Jin, X. Ren, Y. Shen and L. Wang, *Nat. Chem.*, 2023, **15**, 21–32.
21 Q. Li, Q. Chen, P. C. Klauser, M. Li, F. Zheng, N. Wang, X. Li, Q. Zhang, X. Fu, Q. Wang, Y. Xu and L. Wang, *Cell*, 2020, **182**, 85–97.
22 Y. Cheng, J. Wu, Y. Han, J. Xu, Y. Da, Q. Zhao, G. Guo, Y. Zhou, Y. Chen, J. Liu, H. Chen, X. Jiang and X. Cai, *Bioorg. Med. Chem.*, 2021, **42**, 116219.
23 Y. Han, Z. Yang, H. Hu, H. Zhang, L. Chen, K. Li, L. Kong, Q. Wang, B. Liu, M. Wang, J. Lin and P. R. Chen, *J. Am. Chem. Soc.*, 2022, **144**(13), 5702–5707.
24 P. C. Klauser, S. Chopra, L. Cao, K. N. Bobba, B. Yu, Y. Seo, E. Chan, R. R. Flavell, M. J. Evans and L. Wang, *ACS Cent. Sci.*, 2023, DOI: **10.1021/acscentsci.3c00288**.
25 H. Mukherjee, J. Debreczeni, J. Breed, S. Tentarelli, B. Aquila, J. E. Dowling, A. Whitty and N. P. Grimster, *Org. Biomol. Chem.*, 2017, **15**, 9685–9695.
26 Z. Xiang, H. Ren, Y. S. Hu, I. Coin, J. Wei, H. Cang and L. Wang, *Nat. Methods*, 2013, **10**, 885–888.

27 T. Kobayashi, C. Hoppmann, B. Yang and L. Wang, *J. Am. Chem. Soc.*, 2016, **138**, 14832–14835.
28 V. Y. Berdan, P. C. Klauser and L. Wang, *Bioorg. Med. Chem.*, 2021, **29**, 115896.
29 J. Singh, R. C. Petter, T. A. Baillie and A. Whitty, *Nat. Rev. Drug Discovery*, 2011, **10**, 307–317.
30 L. Cao and L. Wang, *Protein Sci.*, 2022, **31**, 312–322.
31 M. Högbom, M. Eklund, P.-A. Nygren and P. Nordlund, *Proc. Natl. Acad. Sci. U. S. A.*, 2003, **100**, 3191–3196.
32 J. Singh, E. M. Dobrusin, D. W. Fry, T. Haske, A. Whitty and D. J. McNamara, *J. Med. Chem.*, 1997, **40**, 1130–1135.
33 K. R. Schmitz, A. Bagchi, R. C. Roovers, M. Paul, P. van Bergen en Henegouwen and K. M. Ferguson, *Structure*, 2013, **21**, 1214–1224.
34 C. Hoppmann and L. Wang, *Chem. Commun.*, 2016, **52**, 5140–5143.
35 O. O. Fadeyi, L. R. Hoth, C. Choi, X. Feng, A. Gopalsamy, E. C. Hett, R. E. Kyne Jr, R. P. Robinson and L. H. Jones, *ACS Chem. Biol.*, 2017, **12**, 2015–2020.
36 B. Yang, N. Wang, P. D. Schnier, F. Zheng, H. Zhu, N. F. Polizzi, A. Ittuveetil, V. Saikam, W. F. DeGrado, Q. Wang, P. G. Wang and L. Wang, *J. Am. Chem. Soc.*, 2019, **141**, 7698–7703.
37 L. H. Jones, *ACS Med. Chem. Lett.*, 2018, **9**, 584–586.
38 M. Nishida, S. Harada, S. Noguchi, Y. Satow, H. Inoue and K. Takahashi, *J. Mol. Biol.*, 1998, **281**, 135–147.
39 J. Liu, S. Li, N. A. Aslam, F. Zheng, B. Yang, R. Cheng, N. Wang, S. Rozovsky, P. G. Wang, Q. Wang and L. Wang, *J. Am. Chem. Soc.*, 2019, **141**, 9458–9462.
40 C. K. V. Nonaka, M. M. Franco, T. Gräf, C. A. de Lorenzo Barcia, R. N. de Ávila Mendonça, K. A. F. de Sousa, L. M. C. Neiva, V. Fosenca, A. V. A. Mendes, R. S. de Aguiar, M. Giovanetti and B. S. de Freitas Souza, *Emerging Infect. Dis.*, 2021, **27**, 1522–1524.
41 Q. Li, J. Wu, J. Nie, L. Zhang, H. Hao, S. Liu, C. Zhao, Q. Zhang, H. Liu, L. Nie, H. Qin, M. Wang, Q. Lu, X. Li, Q. Sun, J. Liu, L. Zhang, X. Li, W. Huang and Y. Wang, *Cell*, 2020, **182**, 1284–1294.
42 G. Nelson, O. Buzko, P. Spilman, K. Niazi, S. Rabizadeh and P. Soon-Shiong, *bioRxiv*, 2021, preprint, DOI: **10.1101/2021.01.13.426558**.
43 F. Tian, B. Tong, L. Sun, S. Shi, B. Zheng, Z. Wang, X. Dong and P. Zheng, *eLife*, 2021, **10**, e69091.
44 D. Planas, T. Bruel, L. Grzelak, F. Guivel-Benhassine, I. Staropoli, F. Porrot, C. Planchais, J. Buchrieser, M. M. Rajah, E. Bishop, M. Albert, F. Donati, M. Prot, S. Behillil, V. Enouf, M. Maquart, M. Smati-Lafarge, E. Varon, F. Schortgen, L. Yahyaoui, M. Gonzalez, J. De Sèze, H. Péré, D. Veyer, A. Sève, E. Simon-Lorière, S. Fafi-Kremer, K. Stefic, H. Mouquet, L. Hocqueloux, S. van der Werf, T. Prazuck and O. Schwartz, *Nat. Med.*, 2021, **27**, 917–924.
45 P. Wang, M. S. Nair, L. Liu, S. Iketani, Y. Luo, Y. Guo, M. Wang, J. Yu, B. Zhang, P. D. Kwong, B. S. Graham, J. R. Mascola, J. Y. Chang, M. T. Yin, M. Sobieszczyk, C. A. Kyratsous, L. Shapiro, Z. Sheng, Y. Huang and D. D. Ho, *Nature*, 2021, **593**, 130–135.
46 S. A. Madhi, V. Baillie, C. L. Cutland, M. Voysey, A. L. Koen, L. Fairlie, S. D. Padayachee, K. Dheda, S. L. Barnabas, Q. E. Bhorat, C. Briner, G. Kwatra, K. Ahmed, P. Aley, S. Bhikha, J. N. Bhiman, A. a. E. Bhorat, J. du Plessis, A. Esmail, M. Groenewald, E. Horne, S.-H. Hwa, A. Jose, T. Lambe, M. Laubscher, M. Malahleha, M. Masenya, M. Masilela, S. McKenzie, K. Molapo, A. Moultrie, S. Oelofse, F. Patel, S. Pillay, S. Rhead, H. Rodel, L. Rossouw, C. Taoushanis, H. Tegally, A. Thombrayil, S. van Eck, C. K. Wibmer, N. M. Durham, E. J. Kelly, T. L. Villafana, S. Gilbert, A. J. Pollard, T. de Oliveira, P. L. Moore, A. Sigal and A. Izu, *N. Engl. J. Med.*, 2021, **384**, 1885–1898.
47 T. Li, H. Cai, H. Yao, B. Zhou, N. Zhang, M. F. van Vlissingen, T. Kuiken, W. Han, C. H. GeurtsvanKessel, Y. Gong, Y. Zhao, Q. Shen, W. Qin, X.-X. Tian, C. Peng, Y. Lai, Y. Wang, C. A. J. Hutter, S.-M. Kuo, J. Bao, C. Liu, Y. Wang, A. S. Richard, H. Raoul, J. Lan, M. A. Seeger, Y. Cong, B. Rockx, G. Wong, Y. Bi, D. Lavillette and D. Li, *Nat. Commun.*, 2021, **12**, 4635.